

# The evolution of phases in FeNiCoCrCuB<sub>x</sub> high entropy alloys produced through microwave sintering and vacuum arc melting

İrem B. Algan Şimşek<sup>a,\*</sup>, Sükrü Talaş<sup>b</sup>, Adem Kurt<sup>a</sup>

<sup>a</sup> Department of Metallurgical and Materials Engineering, Faculty of Technology, Gazi University, Ankara, 06500 Turkey

<sup>b</sup> Department of Metallurgical and Materials Engineering, Faculty of Technology, Afyon Kocatepe University, Afyonkarahisar, 03200 Turkey

(\*Corresponding author: irembalgan@gazi.edu.tr)

Submitted: 25 November 2021; Accepted: 15 March 2022; Available On-line: 12 April 2022

**ABSTRACT:** Microwave heating and sintering techniques are applied to various production lines and material systems to improved their microstructure and mechanical properties in comparison to conventional means of production. These techniques also consume less power and energy compared to conventional heating methods. In this study, the production of high entropy alloys (HEA) by arc melting was carried out with specimens made from compacted and sintered elemental powders; the sintering process of alloy powders prior to remelting prevents certain problems such as porosity and uneven mixing that may occur during casting. We investigated the effects of conventional and microwave sintering processes prior to remelting and casting on structure and properties of FeNiCoCrCuB<sub>x</sub> HEA. Our results show that microwave sintering changes the size and shape of phases and microstructure of the alloy by affecting the liquid-phase separation mechanism. Three-point bending strength and ductility of alloys produced by microwave sintering were superior to conventional sintering.

**KEYWORDS:** Arc melting; High entropy alloys; Liquid phase separation; Microstructure; Microwave sintering

Citation/Citar como: Algan Şimşek, İ. B.; Talaş, S.; Kurt, A. (2022). "The evolution of phases in FeNiCoCrCuB<sub>x</sub> high entropy alloys produced through microwave sintering and vacuum arc melting". *Rev. Metal.* 58(1): e215. <https://doi.org/10.3989/revmetalm.215>

**RESUMEN:** *La evolución de las fases en las aleaciones de alta entropía FeNiCoCrCuB<sub>x</sub> producidas mediante sinterización por microondas y fusión por arco en vacío.* Las técnicas de sinterización y calentamiento por microondas se aplican en varias líneas de producción y materiales para mejorar su microestructura y propiedades mecánicas en comparación con los medios de producción convencionales. Estas técnicas también consumen menos potencia y energía en comparación con los métodos de calentamiento convencionales. En este estudio se realizó la producción de aleaciones de alta entropía (HEA) por fusión de arco con probetas elaboradas a partir de polvos elementales compactados y sinterizados; el proceso de sinterización de los polvos de aleación antes de refundirlos evita ciertos problemas, como la porosidad y la mezcla desigual que pueden ocurrir durante la fundi-

**Copyright:** © 2022 CSIC. This is an open-access article distributed under the terms of the Creative Commons Attribution 4.0 International (CC BY 4.0) License.

ción. Investigamos los efectos de los procesos de sinterización convencionales y por microondas antes de refundir y colar sobre la estructura y las propiedades de un HEA: FeNiCoCrCuBx. Nuestros resultados muestran que la sinterización por microondas cambia el tamaño y la forma de las fases y la microestructura de la aleación al afectar el mecanismo de separación de la fase líquida. La resistencia a la flexión en tres puntos y la ductilidad de las aleaciones producidas por sinterización por microondas fueron superiores a las de la sinterización convencional.

**PALABRAS CLAVE:** Aleaciones de alta entropía; Fusión por arco; Microestructura; Separación de fases líquidas; Sinterización por microondas

**ORCID ID:** İrem B. Algan Şimşek (<https://orcid.org/0000-0001-5206-3722>); Sükrü Talaş (<https://orcid.org/0000-0002-4721-0844>); Adem Kurt (<https://orcid.org/0000-0002-1439-4683>)

## 1. INTRODUCTION

Contrary to conventional alloy models, high entropy alloys (HEA) are obtained by mixing five or more elements in identical or similar proportions and contain simple solid solution phases in the microstructure due to the high mixing entropy effect. Studies until now show that HEAs mostly contain one or more stable solid solution phases and separation can occur in solid solution phases depending on the heat treatment (Pérez *et al.*, 2019). In the synthesis of HEA, many different production methods are employed such as mechanical alloying (solid state), induction melting (liquid state), magnetron sputtering (thin film) and selective laser melting (additive manufacturing), however, vacuum arc melting is a common preferred method (Alshataif *et al.*, 2020). Vacuum arc melting is based on the melting of alloying elements in the form of powder, flakes or pre-alloyed pieces in an inert gas environment (mostly Argon), on a water-cooled copper crucible, with the help of an arc created by non-melting tungsten electrode (Gao *et al.*, 2016). Since the remelting process takes place in a controlled atmosphere, the composition of the alloy being remelted is less affected by the evaporation of some elements during remelting. Thus, metals with high melting points can be remelted easily in a homogeneous manner and the chemical activity of elements such as oxygen and nitrogen in the alloy structure is greatly diminished by the Argon controlled chemical process. This results in an improvement of the microstructural and mechanical properties of the alloy (Zhang *et al.*, 2019; Terentyev *et al.*, 2020). However, during the arc remelting process of powdered alloy, the arc force between the tungsten electrode and the powder material generates evaporated dust particles which tend to scatter, making the remelting process difficult to control due the loss of metal powders and ionization. Compacting and sintering metallic powders prior to vacuum arc melting enables to scale down material loss during remelting and provide more controlled conditions in HEAs (Wu *et al.*, 2021).

The most common method used for sintering powder compacts is conventional sintering (Torralba and Campos, 2014). This involves heating the surface of the powder compact first and then indirectly

the rest of the compact by conduction, convection, and radiation. Therefore, heating and cooling of the compacts depend on the heating and cooling rate of furnace, which usually takes a long time. However, in the microwave sintering technique, which is a relatively new approach in sintering, the powder compacts are heated directly by volumetric heating at the atomic level, and the sintering process can be completed in a shorter time, which is due to the uniform temperature distribution achieved throughout the material. Because of volumetric heating in the microwave, energy consumption for heating is also reduced (Zhou *et al.*, 2018).

CoCrFeMnNi, AlCrCoCuFeNi and similar high entropy alloy systems, which were first studied by Cantor *et al.* (2005), are still being studied extensively (Kao *et al.*, 2009). This is because “transition elements” that make up the alloy system in question have high solubility limits within each other due to similarities in their atomic sizes, melting points and electronegativity, thus facilitating the formation of either single or multiple solid solutions in the microstructure (Fu *et al.*, 2016). Another reason is the low cost of some elements (Fe, Cu etc.) and their ease of availability (Dąbrowa *et al.*, 2017; Fu *et al.*, 2017). Alloy systems consisting of these elements exhibit a dendritic casting structure when they are produced by arc remelting, and with regard to Cu element in the alloy system, copper-rich phases precipitate in the region between dendrites (Kaufman *et al.*, 2018). The tendency of copper to form a second solid solution phase in the structure during solidification is due to its high positive mixture enthalpy ( $\Delta H_{\text{mix}}$ ) compared to other alloying elements, which causes this type of separation. The precipitation of these phases in the microstructure with liquid-phase separation has a significant effect on the deformation and strengthening mechanisms of the alloy, and further studies need to be carried out to address this (Guo *et al.*, 2017; Xian *et al.*, 2018).

In the current study, the sintering process was applied to the samples before casting in order to both reduce material loss during remelting and balance the increase in copper-rich phase size the in microstructure. Then the structural and mechanical effects of conventional and microwave sintering on liquid phase separation during solidification of

FeNiCoCrCuBx high entropy alloys were investigated. The powders forming FeNiCoCrCuBx HEAs were die-compacted and divided into two groups. The main reason why boron is preferred as a minor element in the alloy is that the synergistic effects of boron on solid solution strengthening mechanism and phase transformation (Liu *et al.*, 2016; Algan Şimşek *et al.*, 2021). One group underwent conventional sintering while the other group underwent microwave sintering, followed by arc melting. The specimens were characterized using optical microscopy (Leica DM 4000M), scanning electron microscopy (SEM-Jeol JEM 6060 LV), energy dispersive spectroscopy (EDS), X-ray diffraction (XRD-Bruker D8 Advance), differential scanning calorimetry (DSC-Netzsch/STA 449 F3, Jüpiter), micro hardness (Shimadzu HMV-2) and three-point bending (Instron 3369 Universal testing machine) tests.

## 2. MATERIALS AND METHODS

Powder mixtures were prepared with two different chemical compositions, i.e. FeNiCoCrCuB3 (Alloy A) and FeNiCoCrCuB5 (Alloy B) from Fe, Ni, Co, Cr, Cu and B powders with 99.9% purity and an average size of 300 mesh (approximately 44 µm). The powders were tumble mixed for 30 min in order to ensure homogeneous distribution of the powders. After mixing, the specimens were compacted unidirectionally in a rectangular die of 10×10×55 mm<sup>3</sup> under a pressure of approximately 530 MPa. Conventional or microwave sintering was applied to the compacted HEA prior to arc melting. Conventional sintering process was carried out in a tube furnace with a temperature capacity of 1100 °C under Ar gas atmosphere. Microwave sintering was carried out in an open air atmosphere of a microwave oven with a temperature capacity of 1600 °C, microwave frequency of 2450 MHz (± 25 MHz) and a balanced power support of AC 220 V ± 10 V at 50 Hz. High-stability, long-lifetime continuous industrial microwave generator is used to ensure a continuous and stable running of the system and it has an IR sensor for accurate temperature measurement. The

high-precision IR pyrometer is to measure the temperature directly in the samples. Chemical compositions and sintering parameters of HEAs are given in Table 1. Finally, samples sintered by both methods were remelted three times in an arc remelting furnace in order to ensure chemical homogeneity of the alloy resulting in the production of HEA samples.

Optical microscopy and SEM studies of HEAs were carried out after etching with the aqua regia solution. Energy dispersive spectroscopy (EDS), electron probe micro-analysis (EPMA) and X-ray diffraction (XRD) analyses were carried out to determine the distribution of elements in the microstructure and the crystal structure of the phases present in the microstructure, respectively. The scanning speed and span of XRD device using Cu Kα (λ = 1.5418 Å) cathode was adjusted to 10°/min and between 40° and 80° for 2θ. In order to determine the temperature of phase transitions in HEA, differential scanning calorimetry was performed between 25 °C and 1400 °C at a heating rate of 10 °C·min<sup>-1</sup>. Micro hardness tests of HEAs was carried out with 10 s loading duration and 9.8 N load (HV 2) and ten measurements were taken from each specimens. Three point bending tests were carried out with the help of a universal test machine with a maximum load capacity of 50 kN at a crosshead speed of 1 mm·min<sup>-1</sup> and a support span width of 25.4 mm. HEA alloys were sliced to dimensions of 3×6×30 mm<sup>3</sup> in a wire Electro Discharge Machining device for the three point bending test. Five tests were carried out for each specimen group.

## 3. RESULTS

Sintering and furnace cooling processes of HEA alloys were completed in 415 min (heating speed ≈ 6 °C·min<sup>-1</sup>) with conventional sintering and in 275 min (heating speed ≈ 10 °C·min<sup>-1</sup>) with microwave sintering. The cooling rate of the microwave oven is fast (20 °C·min<sup>-1</sup>) at first, but slower (d ≈ 3 °C·min<sup>-1</sup>) after 600 °C and average cooling rate of conventional oven is 1.4 °C·min<sup>-1</sup>. In contrast to conventional sintering, in microwave sintering the heating of an

TABLE 1. Chemical Compositions (at.-%) and preparation techniques of HEAs

Alloy	Fe	Ni	Co	Cr	Cu	B	Preparation	Sintered temperature (°C)	Sintering time (min)
A1	19.4	19.4	19.4	19.4	19.4	3.0	Conventionally sintered,	980	60
A2							arc melted		
B1	19.0	19.0	19.0	19.0	19.0	5.0	Conventionally sintered,	980	60
B2							arc melted		
							Microwave sintered, arc melted		15

object begins from the center of the sample towards outside. Therefore, uniform heating as well as high density can be achieved in a much shorter time with lower energy consumption compared to conventional sintering (Anklekar *et al.*, 2005). However, the interaction of microwave with materials varies according to their microwave absorption ability. For example, ceramic-based materials can easily convert microwave energy to heat energy as they can absorb microwaves, while metallic materials cannot absorb microwaves and reflect them from the surface due to their opaque nature. For this reason, microwave heating of metallic materials may not be as effective as ceramic materials (Singh *et al.*, 2015; Mishra and Sharma, 2016a). In the current study, the time to rise to sintering temperature in microwave sintering was relatively longer due to the above-mentioned “metal-microwave” interaction, but compared to conventional sintering, the entire processing time was almost half of the duration of conventional sintering.

Density values of conventional and microwave sintered HEAs are given in Fig. 1. The sintered density values were calculated by the ratio of sample weight to actual volume. The densities of Alloy A and Alloy B sintered using microwave were higher than conventionally sintered HEAs. The main reason for the density difference between these alloys, which have the same composition, is that the active diffusion mechanisms in the two sintering techniques are different from each other. Surface diffusion is more dominant in conventional sintering, while grain boundary and bulk diffusions are more dominant in microwave sintering. The number of active diffusion mechanisms in microwave sintering is higher than that in conventional sintering and the diffusion conditions are more uniform due to a well-balanced heat distribution within the specimen. Therefore, the activation energy required for intergranular neck formation during microwave sintering is also lower. Hence, microwave sintering is an advantageous technique in obtaining different

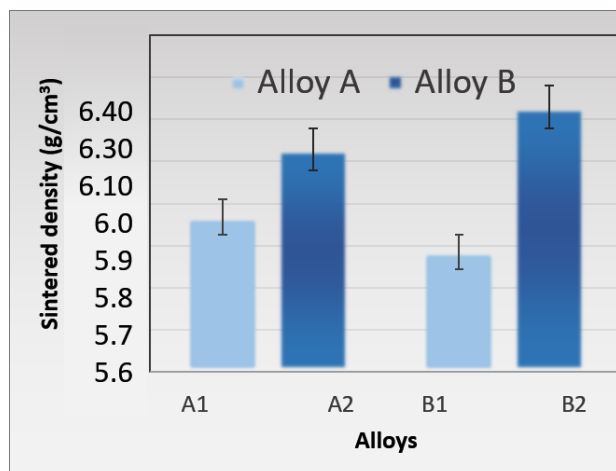


FIGURE 1. Comparison of sintered density of HEAs.

microstructures while increasing the density of parts produced by powder metallurgy (Mishra and Sharma, 2016b).

Figure 2 shows the optical microstructure images of HEAs that were produced by arc melting at 5X magnifications after conventional and microwave sintering. Corroborating data from similar studies in the literature, microstructural images show that all HEA microstructures exhibit a dendritic structure and 3 phases in the dendritic (D) and inter-dendritic (ID) regions occur in the alloys (Zhang *et al.*, 2018; Ferrari *et al.*, 2019; Aguilar-Hurtado *et al.*, 2020). Here, P1 constitutes the dendritic phase, P2 the inter-dendritic phase, while P3 constitutes the orange colored phase located in the ID region. As reported in previous studies, the liquid alloy is divided into two different phases under critical temperatures due to the high positive  $\Delta H_{\text{mix}}$  values of Cu with other elements (Co, Cr, Fe) in Cu-based alloy systems (Wu *et al.*, 2021). In this type of alloys, whose phase diagrams exhibit “monotectic transformation” ( $L1 \rightarrow L2 + \alpha$ ) and a metastable “liquid miscibility gap”, the matrix phase containing Fe-Ni-Co-Cr is separated first from the liquid. Then, in order to reduce the high interfacial energy between the matrix phase, a small amount of Cu-rich phase grows with help of a peritectic ( $L2 + \alpha \rightarrow \beta$ ) reaction by nucleation. At the end of solidification, it takes the form of a precipitate embedded in another phase (Curiotto *et al.*, 2007; Liu *et al.*, 2016). Figure 2 shows that in conventional and microwave sintered HEAs, the P3 phase and the other phases in the microstructure have different morphologies, distributions and ori-

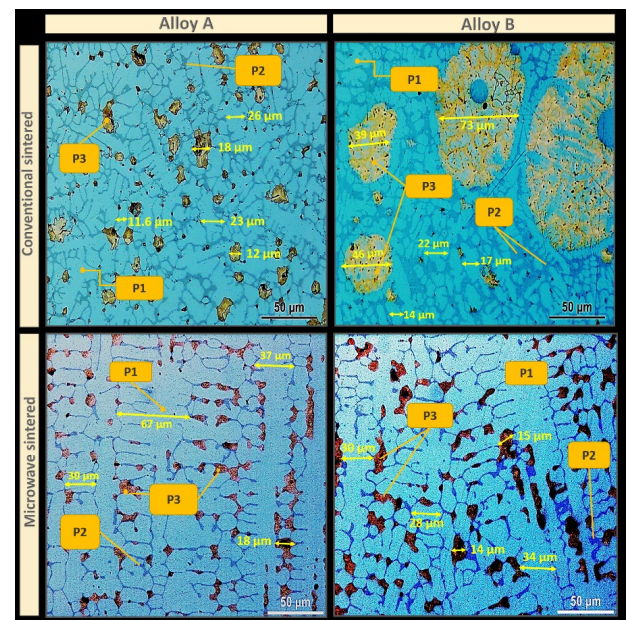


FIGURE 2. Optical microstructures of conventional and microwave sintered HEAs at 50X magnifications. P1 is the dendritic phase, P2 is the inter-dendritic phase, and P3 is the Cu-rich phase (orange colored).

entations. In conventionally sintered HEAs, the dendrite grain structure is irregular, the dendrite grain orientations are different from each other and the size of the P3 phase and ID regions are increasingly coagulated. In microwave-sintered HEAs, however, dendrite sizes were nearly equal and orientations were regular, and the P3 phase was homogeneously spread in the ID regions. It is thought that this co-orientation behavior in the microstructure in A2 and B2 alloys is caused by the rapid volumetric heating in microwave sintering. Because microwave radiation interacts with each of the powder particles in the compacted material at the same time, it creates better mass transport than conventional sintering. The field formed by microwave increases ionic conductivity, and the sintering process can be improved with the high frequency electric field supporting the movement of the cavities on the surface of the powder particles, resulting in well-balanced and featureless microstructures (Oghbaei and Mirzaee, 2010; Zuo *et al.*, 2013).

Additionally, Mishra and Sharma reported that powder metal particles with sizes greater than 100  $\mu\text{m}$  cannot be heated uniformly in microwave heating systems with 2.45 GHz microwave radiation. This is because the depth of the shell, which is the dominant parameter during heating in coarse

metal parts, is responsible for heat generation and absorption of microwave energy, and the rest of the object is heated by conduction (as in conventional heating) from the shell to the inner core (Mishra and Sharma, 2016b). In the current study, the use of metal powder with an average particle size of 300 mesh (approximately 44  $\mu\text{m}$ ) was conducive to the formation of relatively homogeneous microstructures with both A2 and B2 alloys.

The chemical compositions of the phases determined in Fig. 2 are given with standard deviations values in the EDS-EPMA results in Table 2, and the elemental distribution map of Alloy B is given in Fig. 3. We observed that the chemical composition of the P1 phase, which represents the composition of the dendritic region in all HEAs, was rich in Fe-Ni-Co-Cr elements, while the composition of the P2 phase formed in the ID region was richer in Cr and Co (Shivam *et al.*, 2018). In addition, the orange colored second phase (P3) located in ID was rich in Cu element. As it was mentioned above, the P3 phase was formed in the ID region as a result of the liquid-phase separation process that occurred during solidification. As it is seen in Fig. 2, the size of Cu-rich phase increased with the increase in the ratio of boron in the alloy in conventionally sintered A1 and B1 HEAs. For example, the average Cu-rich phase

TABLE 2. Chemical composition (at.-%) of phases in HEAs determined by EDS and EPMA

Sample	Phase	Fe (at.-%)	Ni (at.-%)	Co (at.-%)	Cr (at.-%)	Cu (at.-%)	B (at.-%)
A1	P1	21.5 $\pm$ 4.24	23.3 $\pm$ 2.1	22.9 $\pm$ 2.83	20.9 $\pm$ 2.12	11.1 $\pm$ 2.12	0.1 $\pm$ 0.01
	P2	19.1 $\pm$ 3.54	23.8 $\pm$ 2.8	22.6 $\pm$ 2.12	26.6 $\pm$ 2.12	7.2 $\pm$ 2.8	0.6 $\pm$ 0.11
	P3	3.5 $\pm$ 0.7	5.7 $\pm$ 2.12	4.1 $\pm$ 0	7.7 $\pm$ 0.71	78.5 $\pm$ 1.41	0.4 $\pm$ 0.04
A2	P1	21.2 $\pm$ 1.4	21.3 $\pm$ 2.12	23.3 $\pm$ 0	20.4 $\pm$ 0	13.6 $\pm$ 2.1	0.08 $\pm$ 0.02
	P2	20.0 $\pm$ 0.71	19.8 $\pm$ 1.4	20.1 $\pm$ 2.1	30.4 $\pm$ 2.1	6.6 $\pm$ 0.71	2.8 $\pm$ 0.14
	P3	2.6 $\pm$ 1.4	5.5 $\pm$ 0.71	1.6 $\pm$ 1.41	1.7 $\pm$ 0	87.5 $\pm$ 3.5	1.1 $\pm$ 0.07
B1	P1	24.4 $\pm$ 0.71	21.5 $\pm$ 0	22.7 $\pm$ 0.71	19.2 $\pm$ 0	11.6 $\pm$ 0	0.5 $\pm$ 0.13
	P2	18.5 $\pm$ 0	18.6 $\pm$ 0	23.5 $\pm$ 0.71	26.1 $\pm$ 4.24	11.1 $\pm$ 4.95	2.1 $\pm$ 0.28
	P3	1.5 $\pm$ 0.7	5.1 $\pm$ 0.7	1.5 $\pm$ 1.41	2.4 $\pm$ 0.7	88.1 $\pm$ 2.83	1.3 $\pm$ 0.21
B2	P1	22.2 $\pm$ 0.71	18.7 $\pm$ 1.41	22.8 $\pm$ 0	17.8 $\pm$ 2.12	18.0 $\pm$ 1.41	0.36 $\pm$ 0.07
	P2	20.1 $\pm$ 1.4	17.5 $\pm$ 0.71	20.1 $\pm$ 3.54	33.0 $\pm$ 0	6.0 $\pm$ 5.66	3.2 $\pm$ 0.07
	P3	2.0 $\pm$ 0.71	4.5 $\pm$ 2.12	2.1 $\pm$ 0	1.5 $\pm$ 0	88.5 $\pm$ 3.54	2.0 $\pm$ 0.14

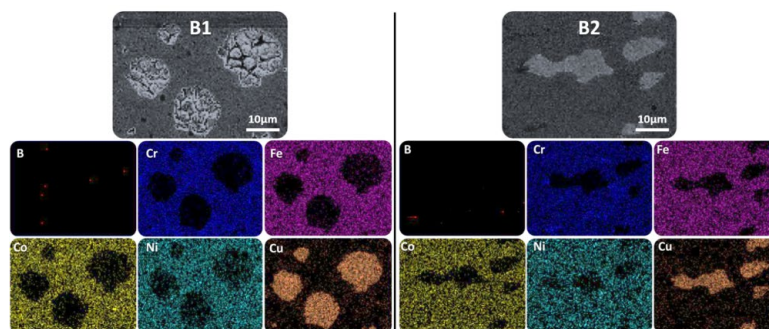


FIGURE 3. SEM and elemental mappings images of B1 and B2 alloys.

size was measured as 15  $\mu\text{m}$  in alloy A1 and 59.5  $\mu\text{m}$  in alloy B1. In nearly all samples, the amount of B in P3, in which Cu and Ni elements were dominant, was lower than the amount of B in the P2 phase where the Cr-Co elements were dominant (Table 2). In other words, the phase that dissolved the most B in the microstructure was the P2 phase located in the ID region. Accordingly, the increase in B in the alloy strongly triggered the separation of the element Cu, which could not be dissolved in other elements and phases from the liquid during solidification, thus causing the volume fraction of P3 phase to increase. However, contrary to this effect observed in conventional sintered HEAs, the average P3 phase size did not change in microwave-sintered HEAs even when the ratio of B was increased (Fig. 2) and in addition average size of P1 increases. Microwave sintering of HEA prior to arc melting significantly changed the composition distribution in the microstructure and the morphology of the phases that while the Cu-rich phase is a spherical in B1 alloy, it is spread between the dendrite grain boundaries in B2 as seen from Fig. 3. Similarly, in a study examining the effect of conventional and microwave sintering in stainless steels (Ertugrul *et al.*, 2015), it was reported that the grain structure in the microstructure of the conventional sintered samples was irregular, while the microwave sintered had a completely recrystallized, featureless and evenly distributed grain structure, which was due to the difference in sintering mechanisms. This suggests that mass flow in conventional sintering was carried out by surface transport mechanism, while in microwave sintering, the volume transport mechanism dominated. In addition, in microwave sintering, the heating is from the center to the outside; the high heating speeds accelerated the diffusion kinetics and reduced the activation energy, fa-

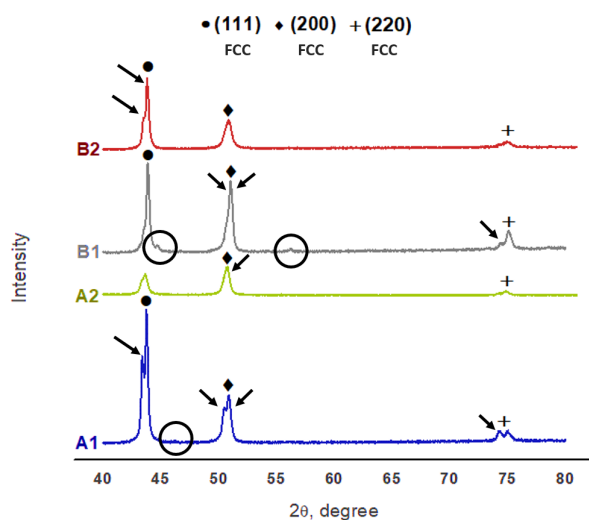


FIGURE 4. XRD patterns of HEAs. Low-intensity peaks observed in alloys A1, B1 and B2, indicated by black arrows, correspond to the  $K\alpha_2$  radiation peaks.

cilitating the nucleation of new grains and providing a more uniform grain formation (Ertugrul, 2014).

Figure 4 shows a comparison of the XRD diffraction patterns in conventional and microwave sintered HEAs. All HEAs produced diffraction peaks at  $43^\circ$ ,  $50^\circ$  and  $74^\circ$ . The P1 phase (111) was seen to be oriented in the planes of the P2 phase (200) and the P3 phase (022). Our calculations suggest that each of the P1, P2 and P3 phases in the microstructure was solid solution phase in the FCC structure, while the lattice parameters varied between 3.57 nm and 3.60 nm. Moreover, low-intensity peaks were observed in alloys A1, A2, B1 and B2 (indicated by the black arrow and circled) in Figure 4. These low-intensity peaks ( $2\theta \approx 51^\circ$  and  $45^\circ$ ) are compatible with the JCPDS-01-077-7712 and JCPDS-01-072-1073 card numbers, respectively (in Fig. 5) and represent the presence of iron chromium boride and copper nickel compounds in the structure. On the other hand, in Fig. 4, it was also observed that the differences in sintering techniques did not cause a significant change in the lattice parameter. Many parameters are used to the possibility to obtain a solid solution phase in the microstructures of HEAs, such as electronegativity difference ( $\chi$ ), enthalpy of mixing ( $\Delta H_{\text{mix}}$ ), atomic size difference ( $\delta$ ), and valence electron concentration (VEC), among which the VEC parameter is most commonly used (Guo and Liu, 2011; Chen *et al.*, 2018). This parameter provides a rough prediction of the possible phases. A VEC value (calculated according to Vegard equation) of lower than 6.87 indicates the formation of a BCC phase in microstructure; when  $6.87 \leq \text{VEC} < 8$ , the formation of FCC + BCC phases is (Chen *et al.*, 2018). In the current study, the calculated VEC value for all HEAs was 7.83, although BCC phase formation was not observed. According to XRD analyses there was three FCC phases occurred in the microstructure. Figure 4 suggests that a difference was detected at the  $2\theta$  peak positions and the planes of the diffraction patterns in the conventional versus the microwave sintered samples while a decrease in peak intensities was observed in A2 and B2 alloys.

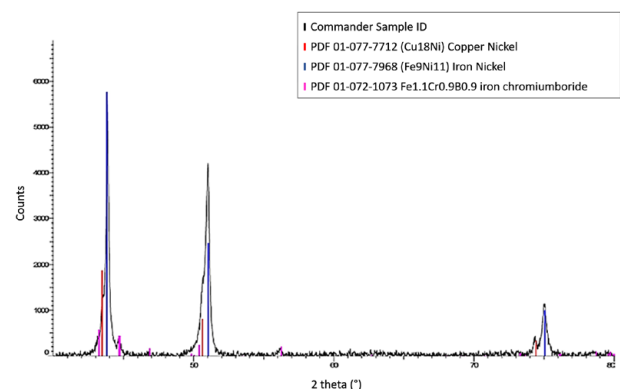


FIGURE 5. JCPDS analysis result of A2 alloy.

Such decreases observed in XRD patterns are often related to crystallite sizes. The fact that microwave sintering creates a more homogeneous and equi-sized dendrite grain structure in HEA's is believed to cause a decrease in peak intensity by changing the fraction and/or size of crystal structures.

The current JCPDS (Joint Committee on Powder Diffraction Standards) card analysis for A2 alloy is shown in Fig. 5. We predicted that the chemical compositions of the solid solution phases in the microstructure could only be Cu<sub>19</sub>Ni, Fe<sub>9</sub>Ni<sub>11</sub> and Fe<sub>1.1</sub>Cr<sub>0.9</sub>B<sub>0.9</sub>. However, we observed the absence of a one-to-one match in the values of peak intensities (relative intensity of peaks). This indicates that the JCPDS analysis was not sufficient in determining the new and complex structure of HEAs in the current study.

Figure 6 shows the DSC analyses of Alloy A and Alloy B generated by conventional and microwave sintering. These analyses were performed in three steps to determine the thermal stability and phase development. Examination of the first heating curves show the presence of a transformation at around 1120 °C. This temperature has been reported to the represent melting point of Cu-rich phases in the ID region precipitate (Tariq *et al.*, 2013; Jones *et al.*, 2015). The phase transformation curves of HEAs show the presence of three endothermic peaks in conventionally sintered A1 and B1 alloys and two endothermic peaks in microwave-sintered A2 and B2 alloys. This suggests that the dendrite phase solidification was completed in one step in

A2 and B2 alloys at around 1350 °C and 1365 °C, while in A1 and B1 alloys the transformations took place in two stages. The small peaks in alloys A1 and B1 indicate that the alloys underwent a weak phase transformation (Shivam *et al.*, 2018). This thermal shift was seen to disappear in A2 and B2 alloys with the use of microwave sintering. Yet, another difference between the curves is that the aforementioned transformation temperatures were shifted to higher temperatures in A2 and B2 alloys sintered with microwave. When all these effects are taken into consideration, it can be said that microwave sintering plays an important part in the solidification of phases, and the volumetric heating effect causes phase transformations to occur at higher temperatures, which are more stable and occur in a single step. Cooling curves are similar to the first heating process, three different transformations were observed in A1 and B1 alloys and the peak intensities of the second transformation increased significantly in A2 and B2 alloys because of volumetric heating at the atomic level. Finally, the second heating curve shows that the structure in alloy A1 became more stable due to reheating and exhibited two transformations. The purpose of the second heating was to eliminate the already unstable phase transformations and to observe the transformation more clearly; it may also trigger the appearance of phases that tend to grow.

The hardness and bending strength of HEAs is given in Fig. 7. According to Fig. 7a, increasing the B content increases the hardness of the alloy because of solid solution hardening effect. The solid

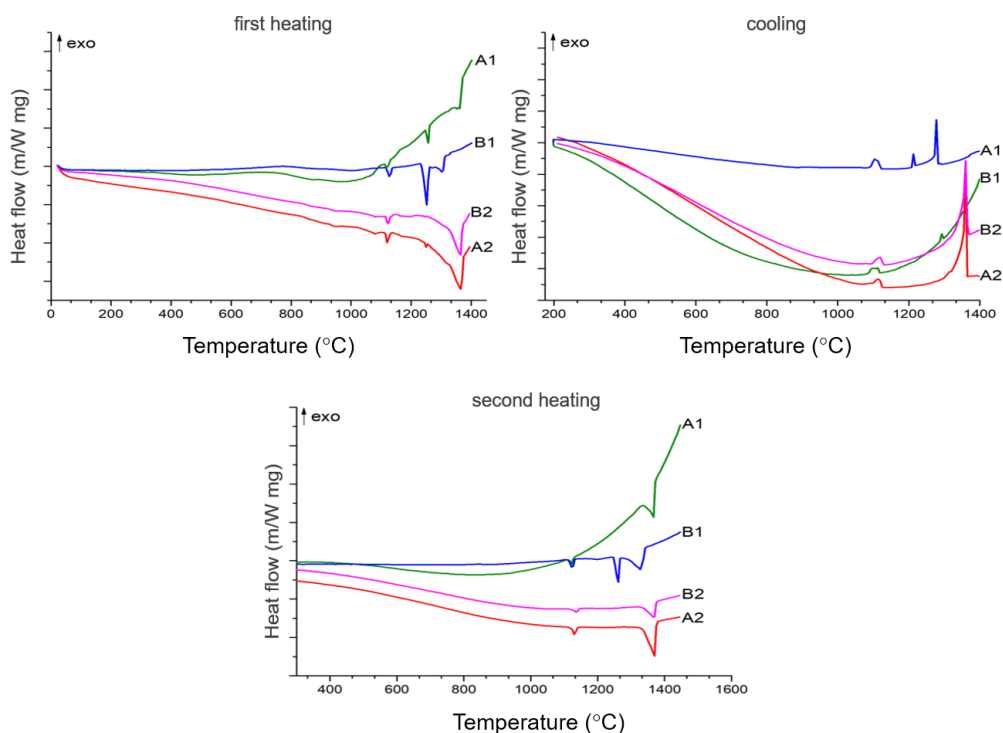


FIGURE 6. DSC curves of HEAs: first heating, cooling and second heating

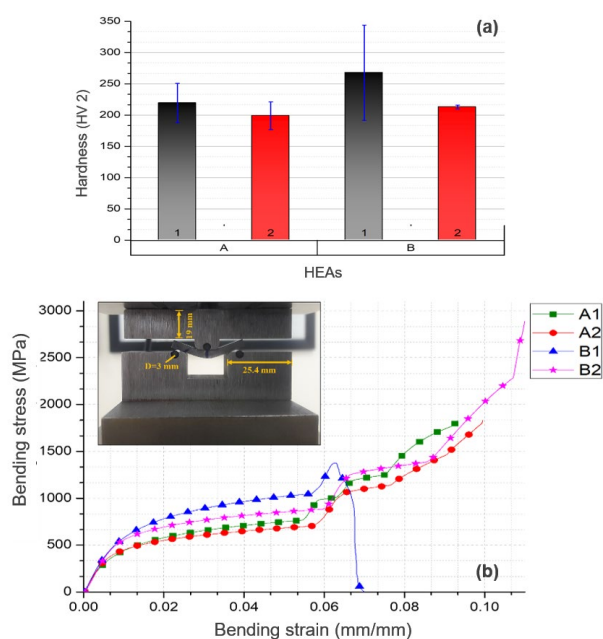


FIGURE 7. Mechanical properties of HEAs: the hardness (a) and three-point bending stress-bending strain curves (b) of HEAs.

solution hardening effect formed by solid solution of B and this situation makes the dislocation movements difficult (Savaşkan and Hekimoğlu, 2014; Hekimoğlu *et al.*, 2019). On the other hand, the microwave sintered A2 and B2 alloys have lower hardness values than the conventionally sintered A1 and B1 alloys. Figure 2 clearly shows that the morphology and distribution of the Cu-rich P3 phase changed with microwave sintering. The phase volume-ratios of the “P2+P3” (inter dendritic) phase was calculated from the optical images in Fig. 2 and the results show that B1 has the highest ratio which is 54.4%, B2 has 26.3%, A1 has 23.7 and A2 has the lowest ratio which is 14.7%. On the other hand, the best results obtained in three-point bending tests repeated five times for each group are given in Fig. 7.b. As it can be seen from the Fig. 7b, the three-point bending strength and bending elongation of conventionally sintered HEAs decreased with the increasing the B content. The EDS-EPMA data given in Table 2 suggests that this may be caused by metal-borides detected in the JCPDS card due to an increased solubility of B in the ID regions. The increase in the B amount in the alloy triggered the precipitation of the P3 phase by causing the solute enrichment as a result of the structural super cooling. The low solubility of B element in Cu compared to the B-Cu binary phase diagrams, which is more soluble in the ID region, caused the P3 phase to increase in size, which was rejected from the liquid during solidification (Chandravanshi *et al.*, 2010; Hou *et al.*, 2019). Although this effect in the P3 phase led to

TABLE 3. Average bending strength and bending strain values of HEAs with standard deviation

Alloy	Bending strength (MPa)	Bending strain (mm·mm <sup>-1</sup> )
A1	1820 ± 11.06	0.08 ± 0.005
A2	1789 ± 9.52	0.09 ± 0.009
B1	1332 ± 8.04	0.06 ± 0.002
B2	2832 ± 7.87	0.10 ± 0.004

an increase in the hardness values of the conventionally sintered B1 alloy, it reduced its three-point bending strength. In addition, as it can be seen from the phase-volume ratios mentioned above, microwave sintering significantly affected the distribution of phases in the microstructure. This compositional and morphological change occurring in the D and ID phases caused significant differences in the mechanical properties of HEAs.

Average bending strength and strain values of HEAs were given in Table 3. According to results the strain values of Alloy A were slightly improved by providing faster and homogeneous heating with microwave sintering (Singh *et al.*, 2015). On the other hand, the strength of microwave sintered B2 alloy was increased considerably that of the conventional sintered B1 alloy, and a significant improvement in ductility was achieved. According to these results, microwave sintering improve strength and ductility by eliminating brittleness caused by the increase in Boron content in the microstructure is thought.

#### 4. CONCLUSIONS

The findings of the current study on the effects of conventional and microwave sintering on solidification, microstructure and mechanical properties of FeNiCoCrCuBx high entropy alloys produced by arc melting can be summarized as follows:

- The liquid-phase separation process that occurred during solidification of FeNiCoCrCuBx HEAs, which exhibit a dendritic microstructure, was modified by the effect of microwave sintering. While the microwave sintering did not affect the type and number of phases formed in the microstructure, it especially had significant effects on the size, morphology and distribution of the P3 phase.
- Transport mechanisms between the powder grains during sintering was comparatively different for different sintering techniques. Therefore this situation changed the casting solidification dynamics of HEAs.
- Unlike conventionally sintered A1 and B1 alloys, microwave sintering yielded a more regular microstructure, homogeneous distribution of phases and dendrite grains.

- Although the hardness values of microwave-sintered HEAs was lower than conventional sintered HEAs, their strength and ductility properties improved significantly. The strength of B2, which was microwave treated, was twice that of B1 (2830 MPa).
- The microwave sintering in the production of HEAs by arc melting significantly affected the solidification processes and rearranged the microstructure. While this change in the microstructure slightly decreased the hardness of HEAs, it caused an increase in the three-point bending strength. Sintering with microwave before casting can enable the production of materials, which would show a more homogenous microstructure at a lower cost by saving time and energy.

## ACKNOWLEDGMENTS

This work was funded by Gazi University Scientific Research Projects Unit (no. 07/2018-07) and National Boron Research Institute (BOREN). The authors also would like to thank to Muhammed Nasuh ARIK from BOREN for technical support in the current study.

## REFERENCES

- Aguilar-Hurtado, J.Y., Vargas-Uscategui, A., Paredes-Gil, K., Palma-Hillerns, R., Tobar, M.J., Amado, J.M. (2020). Boron Addition in a Non-Equiatomic Fe<sub>50</sub>Mn<sub>30</sub>Co<sub>10</sub>Cr<sub>10</sub> Alloy Manufactured by Laser Cladding: Microstructure and Wear Abrasive Resistance. *Appl. Surf. Sci.* 515, 146084. <https://doi.org/10.1016/j.apsusc.2020.146084>.
- Algan Şimşek, İ.B., Arık, M.N., Talaş, Ş., Kurt, A. (2021). The Effect of B Addition on the Microstructural and Mechanical Properties of FeNiCoCrCu High Entropy Alloys. *Metall. Mater. Trans. A*: 52 (5), 1749-1758. <https://doi.org/10.1007/s11661-021-06186-9>.
- Alshataif, Y.A., Sivasankaran, S., Al Mufadi, F.A., Alaboodi, A.S., Ammar, H.R. (2020). Manufacturing methods, microstructural and mechanical properties evolutions of high entropy alloys: a review. *Met. Mater. Int.* 26, 1099-1133. <https://doi.org/10.1007/s12540-019-00565-z>.
- Anklekar, R.M., Bauer, K., Agrawal, D.K., Roy, R. (2005). Improved Mechanical Properties and Microstructural Development of Microwave Sintered Copper and Nickel Steel PM Parts. *Powder Metall.* 48 (1), 39–46. <https://doi.org/10.1179/003258905X37657>.
- Cantor, B., Audebert, F., Galano, M., Kim, K.B., Stone, I.C., Warren, P.J. (2005). Novel Multicomponent Alloys. *J. Metastable Nanocryst. Mater.* 24-25, 1-6. <https://doi.org/10.4028/www.scientific.net/JMN.24-25.1>.
- Chandravanshi, V.K., Sarkar, R., Ghosal, P., Kamat, S.V., Nandy, T.K. (2010). Effect of Minor Additions of Boron on Microstructure and Mechanical Properties of As-Cast near  $\alpha$  Titanium Alloy. *Metall. Mater. Trans. A*: 41 (4), 936–946. <https://doi.org/10.1007/s11661-009-0155-0>.
- Chen, R., Qin, G., Zheng, H., Wang, L., Su, Y., Chiu, Y.L., Ding, H., Guo, J., Fu, H. (2018). Composition Design of High Entropy Alloys Using the Valence Electron Concentration to Balance Strength and Ductility. *Acta Mater.* 144, 129–137. <https://doi.org/10.1016/j.actamat.2017.10.058>.
- Curiotto, S., Greco, R., Pryds, N.H., Johnson, E., Battezzati, L. (2007). The Liquid Metastable Miscibility Gap in Cu-Based Systems. *Fluid Ph. Equilibria* 256 (1–2), 132–136. <https://doi.org/10.1016/j.fluid.2006.10.003>.
- Dąbrowa, J., Cieślak, G., Stygar, M., Mroczka, K., Berent, K., Kulik, T., Danielewski, M. (2017). Influence of Cu Content on High Temperature Oxidation Behavior of AlCoCrCuFeNi High Entropy Alloys (x = 0; 0.5; 1). *Intermetallics* 84, 52–61. <https://doi.org/10.1016/j.intermet.2016.12.015>.
- Ertugrul, Onur (2014). Production of Ceramic Reinforced Stainless Steel Matrix Composites by Conventional and Microwave Sintering Methods. Dokuz Eylül University.
- Ertugrul, O., Park, H.-S., Onel, K., Willert-Porada, M. (2015). Structure and Properties of SiC and Emery Powder Reinforced PM 316l Matrix Composites Produced by Microwave and Conventional Sintering. *Powder Metall.* 58 (1), 41–50. <https://doi.org/10.1179/1743290114Y.0000000100>.
- Ferrari, V., Wolf, W., Zepon, G., Coury, F.G., Kaufman, M.J., Bolfarini, C., Kiminami, C.S., Botta, W.J. (2019). Effect of Boron Addition on the Solidification Sequence and Microstructure of AlCoCrFeNi Alloys. *J. Alloys Compd.* 775, 1235–1243. <https://doi.org/10.1016/j.jallcom.2018.10.268>.
- Fu, Z., Chen, W., Wen, H., Zhang, D., Chen, Z., Zheng, B., Zhou, Y., Lavernia, E.J. (2016). Microstructure and Strengthening Mechanisms in an FCC Structured Single-Phase Nanocrystalline Co<sub>25</sub>Ni<sub>12.5</sub>Fe<sub>25</sub>Al<sub>7.5</sub>Cu<sub>17.5</sub> High-Entropy Alloy. *Acta Mater.* 107, 59–71. <https://doi.org/10.1016/j.actamat.2016.01.050>.
- Fu, X., Schuh, C.A., Olivetti, E.A. (2017). Materials Selection Considerations for High Entropy Alloys. *Scr. Mater.* 138, 145–150. <https://doi.org/10.1016/j.scriptamat.2017.03.014>.
- Gao, M.C., Yeh, J.-W., Liaw, P.K., Zhang, Y. (2016). *High-Entropy Alloys. Fundamentals and Applications*. Springer, Cham. <https://doi.org/10.1007/978-3-319-27013-5>.
- Guo, S., Liu, C.T. (2011). Phase Stability in High Entropy Alloys: Formation of Solid-Solution Phase or Amorphous Phase. *Pro. Nat. Sci.: Mater. Int.* 21 (6), 433–446. [https://doi.org/10.1016/S1002-0071\(12\)60080-X](https://doi.org/10.1016/S1002-0071(12)60080-X).
- Guo, T., Li, J., Wang, J., Wang, Y., Kou, H., Niu, S. (2017). Liquid-Phase Separation in Undercooled CoCrCuFeNi High Entropy Alloy. *Intermetallics* 86, 110–115. <https://doi.org/10.1016/j.intermet.2017.03.021>.
- Hekimoğlu, A.P., Turan, Y.E., İsmailoğlu, I., Akyol, M.E., Şen, E. (2019). Effect of Grain Refinement with Boron on the Microstructure and Mechanical Properties of Al-30Zn Alloy. *J. Fac. Eng. Archit. Gazi Univ.* 34 (1), 523–534. <https://doi.org/10.17341/gazimmfd.416512>.
- Hou, L., Hui, J., Yao, Y., Chen, J., Liu, J. (2019). Effects of Boron Content on Microstructure and Mechanical Properties of AlFeCoNiBx High Entropy Alloy Prepared by Vacuum Arc Melting. *Vacuum* 164, 212–218. <https://doi.org/10.1016/j.vacuum.2019.03.019>.
- Jones, N.G., Christofidou, K.A., Stone, H.J. (2015). Rapid Precipitation in an Al<sub>75</sub>CrFeCoNiCu High Entropy Alloy. *Mater. Sci. Technol.* 31 (10), 1171–1177. <https://doi.org/10.1179/1743284715Y.0000000004>.
- Kao, Y.F., Chen, T.J., Chen, S.K., Yeh, J.W. (2009). Microstructure and Mechanical Property of As-Cast, -Homogenized, and -Deformed AlxCoCrFeNi (0 ≤ x ≤ 2) High-Entropy Alloys. *J. Alloys Compd.* 488 (1), 57–64. <https://doi.org/10.1016/j.jallcom.2009.08.090>.
- Kaufman, M.J., Munitz, A., Nahmany, M., Derimow, N., Abbaschian, R. (2018). Microstructure and Mechanical Properties of Heat Treated Al<sub>1.25</sub>CoCrCuFeNi High Entropy Alloys. *Mater. Sci. Eng. A* 714, 146–159. <https://doi.org/10.1016/j.msea.2017.12.084>.
- Liu, X., Lei, W., Ma, L., Liu, J., Liu, J., Cui, J. (2016). Effect of Boron on the Microstructure, Phase Assemblage and Wear Properties of Al<sub>0.5</sub>CoCrCuFeNi High-Entropy Alloy. *Rare Metal. Mat. Eng.* 45 (9), 2201–2207. [https://doi.org/10.1016/s1875-5372\(17\)30003-6](https://doi.org/10.1016/s1875-5372(17)30003-6).
- Mishra, R.R., Sharma, A.K. (2016a). A Review of Research Trends in Microwave Processing of Metal-Based Materials and Opportunities in Microwave Metal Casting. *Crit. Rev. Solid State Mater. Sci.* 41 (3), 217–255. <https://doi.org/10.1080/10408436.2016.1142421>.
- Mishra, R.R., Sharma, A.K. (2016b). Microwave-Material Interaction Phenomena: Heating Mechanisms, Challenges

- and Opportunities in Material Processing. *Compos-A: App. Sci. Manuf.* 81, 78–97. <https://doi.org/10.1016/j.compositesa.2015.10.035>.
- Oghbaei, M., Mirzaee, O. (2010). Microwave versus Conventional Sintering: A Review of Fundamentals, Advantages and Applications. *J. Alloys Compd.* 494 (1–2), 175–189. <https://doi.org/10.1016/j.jallcom.2010.01.068>.
- Pérez, P., Garcés, G., Frutos-Myro, E., Antoranz, J.M., Tsipas, S., Adeva, P. (2019). Design and Characterization of Three Light-Weight Multi-Principal-Element Alloys Potentially Candidates as High-Entropy Alloys. *Rev. Metal.* 55 (3), e147. <https://doi.org/10.3989/revmetalm.147>.
- Savaşkan, T., Hekimoğlu, A.P. (2014). Microstructure and Mechanical Properties of Zn-15Al-Based Ternary and Quaternary Alloys. *Mater. Sci. Eng. A* 603, 52–57. <https://doi.org/10.1016/j.msea.2014.02.047>.
- Shivam, V., Basu, J., Pandey, V.K., Shadangi, Y., Mukhopadhyay, N.K. (2018). Alloying Behaviour, Thermal Stability and Phase Evolution in Quinary AlCoCrFeNi High Entropy Alloy. *Adv. Powder Technol.* 29 (9), 2221–2230. <https://doi.org/10.1016/j.apt.2018.06.006>.
- Singh, S., Gupta, D., Jain, V., Sharma, A.K. (2015). Microwave Processing of Materials and Applications in Manufacturing Industries: A Review. *Mater. Manuf. Process.* 30 (1), 1–29. <https://doi.org/10.1080/10426914.2014.952028>.
- Tariq, N.H., Naeem, M., Hasan, B.A., Akhter, J.I., Siddique, M. (2013). Effect of W and Zr on Structural, Thermal and Magnetic Properties of AlCoCrCuFeNi High Entropy Alloy. *J. Alloys Compd.* 556, 79–85. <https://doi.org/10.1016/j.jallcom.2012.12.095>.
- Terentyev, D., Khvan, T., You, J.-H., Van Steenberghe, N. (2020). Development of Chromium and Chromium-Tungsten Alloy for the Plasma Facing Components: Application of Vacuum Arc Melting Techniques. *Journal of Nuclear Materials* 536, 152204. <https://doi.org/10.1016/j.jnucmat.2020.152204>.
- Torralba, J.M., Campos, M. (2014). Toward High Performance in Powder Metallurgy. *Rev. Metal.* 50 (2), e017. <https://doi.org/10.3989/revmetalm.017>.
- Wu, M.-W., Fu, Y.C., Lin, Y.-L., Lin, C.-Y. Chen, C.-S. (2021). Promoting the Sintering Densification and Mechanical Properties of Gas-Atomized High-Entropy Alloy Powder by Adding Boron. *Mater. Charact.* 179, 111370. <https://doi.org/10.1016/j.matchar.2021.111370>.
- Xian, X., Lin, L., Zhong, Z., Zhang, C., Chen, C., Song, K., Cheng, J., Wu, Y. (2018). Precipitation and Its Strengthening of Cu-Rich Phase in CrMnFeCoNiCu High-Entropy Alloys. *Mater. Sci. Engine A* 713, 134–40. <https://doi.org/10.1016/j.msea.2017.12.060>.
- Zhang, W., Liaw, P.K., Zhang, Y. (2018). Science and Technology in High-Entropy Alloys. *Sci. China Mater.* 61 (1), 2–22. <https://doi.org/10.1007/s40843-017-9195-8>.
- Zhang, H., Wang, C., Xu, P., Limberg, W., Willumeit-Römer, R., Pyczak, F., Ebel, F. (2019). Novel Type of Biomedical Titanium-Manganese-Niobium Alloy Fabricated by Metal Injection Moulding. Euro PM 2019 Congress and Exhibition.
- Zhou, C., Li, L., Wang, J., Yi, J., Peng, Y. (2018). A Novel Approach for Fabrication of Functionally Graded W/Cu Composites via Microwave Processing. *J. Alloys Compd.* 743, 383–387. <https://doi.org/10.1016/j.jallcom.2018.01.372>.
- Zuo, F., Carry, C., Saunier, S., Marinel, S., Goeuriot, D. (2013). Comparison of the Microwave and Conventional Sintering of Alumina: Effect of MgO Doping and Particle Size. *J. Am. Ceram. Soc.* 96 (6), 1732–1737. <https://doi.org/10.1111/jace.12320>.